View metadata, citation and similar papers at core.ac.uk

brought to you by CORE

provided by Open Repository and Bibliography - Luxembourg

Neurobiology of Disease 89 (2016) 112–125

Contents lists available at ScienceDirect

Neurobiology of Disease

journal homepage: www.elsevier.com/locate/ynbdi

Loss of DJ-1 impairs antioxidant response by altered glutamine and serine metabolism

J. Meiser [a], S. Delcambre [a], A. Wegner [a], C. Jäger [a], J. Ghelfi [a], A. Fouquier d'Herouel [a], X. Dong [a], D. Weindl [a], C. Stautner [c], Y. Nonnenmacher [a], A. Michelucci [a,k], O. Popp [j], F. Giesert [c], S. Schildknecht [b], L. Krämer [a], J.G. Schneider [a,i], D. Woitalla [g], W. Wurst [c,d,e,f], A. Skupin [a,h], D.M. Vogt Weisenhorn [c], R. Krüger [a], M. Leist [b], K. Hiller [a,*]

[a] Luxembourg Centre for Systems Biomedicine, University of Luxembourg, L-4367 Belvaux, Luxembourg
[b] Doerenkamp-Zbinden Chair for In Vitro Toxicology and Biomedicine, University of Konstanz, Konstanz D-78457, Germany
[c] Helmholtz Zentrum München, German Research Center for Environmental Health, Institute of Developmental Genetics, Ingolstädter Landstr. 1, 85764 Neuherberg, Germany
[d] Deutsches Zentrum für Neurodegenerative Erkrankungen e. V. (DZNE) Standort München, Feodor-Lynen-Strasse 17, 81377 München, Germany
[e] Munich Cluster for Systems Neurology (SyNergy), Adolf-Butenandt-Institut, Ludwig-Maximilians-Universität München, Schillerstrasse 44, 80336 München, Germany
[f] Technische Universität München-Weihenstephan, Lehrstuhl für Entwicklungsgenetik, c/o Helmholtz Zentrum München, Ingolstädter Landstr. 1, 85764 Neuherberg, Germany
[g] Neurology, St. Josef Hospital, Ruhr-University, Gudrunstr. 56, 44780 Bochum, Germany
[h] National Center for Microscopy and Imaging Research, University of California San Diego, La Jolla, CA, United States
[i] Saarland University Medical Center, Department of Internal Medicine II, Homburg/Saar, Germany
[j] Mass Spectrometry Core Facility, Max-Delbrueck Center for Molecular Medicine, Robert-Roessle Strasse 10, 13125 Berlin, Germany
[k] NorLux Neuro-Oncology Laboratory, Luxembourg Institute of Health, 84, Val Fleuri, L-1526, Luxembourg

ARTICLE INFO

Article history:
Received 17 July 2015
Revised 16 January 2016
Accepted 20 January 2016
Available online 1 February 2016

Keywords:
Parkinson's disease
Mitochondrial metabolism
Glutamine
Serine
Folate mediated one-carbon metabolism
Oxidative stress
ROS
Glutathione
Stable isotope-assisted metabolomics
GC/MS

ABSTRACT

The oncogene *DJ-1* has been originally identified as a suppressor of PTEN. Further on, loss-of-function mutations have been described as a causative factor in Parkinson's disease (PD). DJ-1 has an important function in cellular antioxidant responses, but its role in central metabolism of neurons is still elusive. We applied stable isotope assisted metabolic profiling to investigate the effect of a functional loss of DJ-1 and show that DJ-1 deficient neuronal cells exhibit decreased glutamine influx and reduced serine biosynthesis. By providing precursors for GSH synthesis, these two metabolic pathways are important contributors to cellular antioxidant response. Down-regulation of these pathways, as a result of loss of DJ-1 leads to an impaired antioxidant response. Furthermore, DJ-1 deficient mouse microglia showed a weak but constitutive pro-inflammatory activation. The combined effects of altered central metabolism and constitutive activation of glia cells raise the susceptibility of dopaminergic neurons towards degeneration in patients harboring mutated *DJ-1*. Our work reveals metabolic alterations leading to increased cellular instability and identifies potential new intervention points that can further be studied in the light of novel translational medicine approaches.

© 2016 The Authors. Published by Elsevier Inc. This is an open access article under the CC BY-NC-ND license (http://creativecommons.org/licenses/by-nc-nd/4.0/).

1. Introduction

DJ-1 (*PARK 7*) is expressed in different organs throughout the body and has first been identified as an oncogene together with activated Ras (Nagakubo et al., 1997). High levels of DJ-1 have been associated with malignancy of tumor development (Nagakubo et al., 1997; Davidson et al., 2008; Kim et al., 2005; Yuen et al., 2008). Mechanistically, DJ-1 has been identified as a repressor of the phosphatase PTEN, which itself is a repressor of PKB/AKT (Stambolic et al., 1998; Sun et al., 1999). In case of *DJ-1* overexpression, PKB/AKT is hyperphosphorylated, promoting cell survival and anaplerotic metabolism needed for proliferation (Kim et al., 2005). In cancer cells, DJ-1 has been identified as a positive regulator of NRF2 (Clements et al., 2006), a master regulator in the antioxidant response. NRF2 has also been shown to influence central metabolism (Hayes and Dinkova-Kostova, 2014). However, its role in neuronal metabolism remains to be elucidated. While *DJ-1* overexpression provokes oncogenesis, loss of function mutations in *DJ-1* have been associated with a familial autosomal recessive form of Parkinson's disease (PD) with an early onset of disease progression (Bonifati, 2003; Bonifati et al., 2003; Van Duijn et al., 2001). PD leads to motor and non-motor symptoms with hallmarks such as

* Corresponding author at: University of Luxembourg, Luxembourg Centre for Systems Biomedicine, 6, avenue du Swing, L-4367 Belvaux, Luxembourg.
E-mail address: karsten.hiller@uni.lu (K. Hiller).
Available online on ScienceDirect (www.sciencedirect.com).

http://dx.doi.org/10.1016/j.nbd.2016.01.019
0969-9961/© 2016 The Authors. Published by Elsevier Inc. This is an open access article under the CC BY-NC-ND license (http://creativecommons.org/licenses/by-nc-nd/4.0/).

elevated levels of reactive oxygen species (ROS) and specifically, a decay of dopaminergic (DAergic) neurons of the *substantia nigra pars compacta* (Antony et al., 2013).

Lack of DJ-1 hampers quenching of cellular ROS, affecting mitochondrial and cellular integrity (Clements et al., 2006; Ariga et al., 2013; Irrcher et al., 2010; Kahle et al., 2009; Krebiehl et al., 2010). Within the brain, *DJ-1* is expressed in neuronal as well as non-neuronal cells (Bader et al., 2005) and is up-regulated with increasing oxidative stress (Baulac et al., 2009). Oxidation of cysteine residues in DJ-1 leads to a shift of the isoelectric point (pI) and subsequent relocation of the protein to the nucleus, as well as the mitochondrial membrane (Canet-Avilés et al., 2004). ROS production and a concomitant shift of the pI have also been shown in cells exposed to lipopolysaccharide (LPS), an inducer of inflammatory responses (Mitsumoto and Nakagawa, 2001) indicating further implications in the context of neuroinflammation and mitochondrial metabolism (Kim et al., 2013; Trudler et al., 2014; Waak et al., 2009). Activation of microglia has been found to correlate with the occurrence of neurodegenerative diseases (Brown and Neher, 2010; Meiser et al., 2013).

Although there is evidence that DJ-1 regulates metabolism directly (Lee et al., 2012) and indirectly (Clements et al., 2006; Aleyasin et al., 2010; van der Brug et al., 2008), a detailed understanding of its role in central metabolism, especially in the context of PD, is still missing.

Here, we investigated the impact of a functional loss of DJ-1 on cellular metabolism. Our study demonstrates that loss of DJ-1 affects central metabolism by decreasing glutamine influx and serine biosynthesis. These two metabolic pathways provide the precursors glutamate, serine and glycine for *de novo* synthesis of glutathione. In line with these metabolic flux changes, we observed decreased glutathione levels in DJ-1 deficient cells.

Additionally, DJ-1 deficient mouse microglia showed a weak but constitutive pro-inflammatory phenotype. We reason that the combination of weak pro-inflammatory activation with metabolic dysfunction renders DAergic neurons more susceptible for early cell death.

2. Results

2.1. Loss of DJ-1 increases susceptibility to oxidative stress

To investigate the effect of loss of DJ-1 on central metabolism, we targeted *DJ-1* by RNAi in the human tyrosine hydroxylase (TH)-positive neuronal cell model LUHMES (Scholz et al., 2011) (Fig. 1a and b; S1). As a control we used non-specific *shRNA* and generated *shCtrl* LUHMES cells in parallel to the *shDJ-1* cells. LUHMES cells are conditionally immortalized and are postmitotic after differentiation (Scholz et al., 2011).

To confirm our working hypothesis that *DJ-1* deficient cells are more susceptible to oxidative stress (Zhou and Freed, 2005), we first performed a viability assay after treating the cells with different concentrations of the ROS-inducing compound 6-hydroxydopamine (6-OHDA) (Fig. 1c). 6-OHDA treated LUHMES cells lacking DJ-1 showed 30–40%

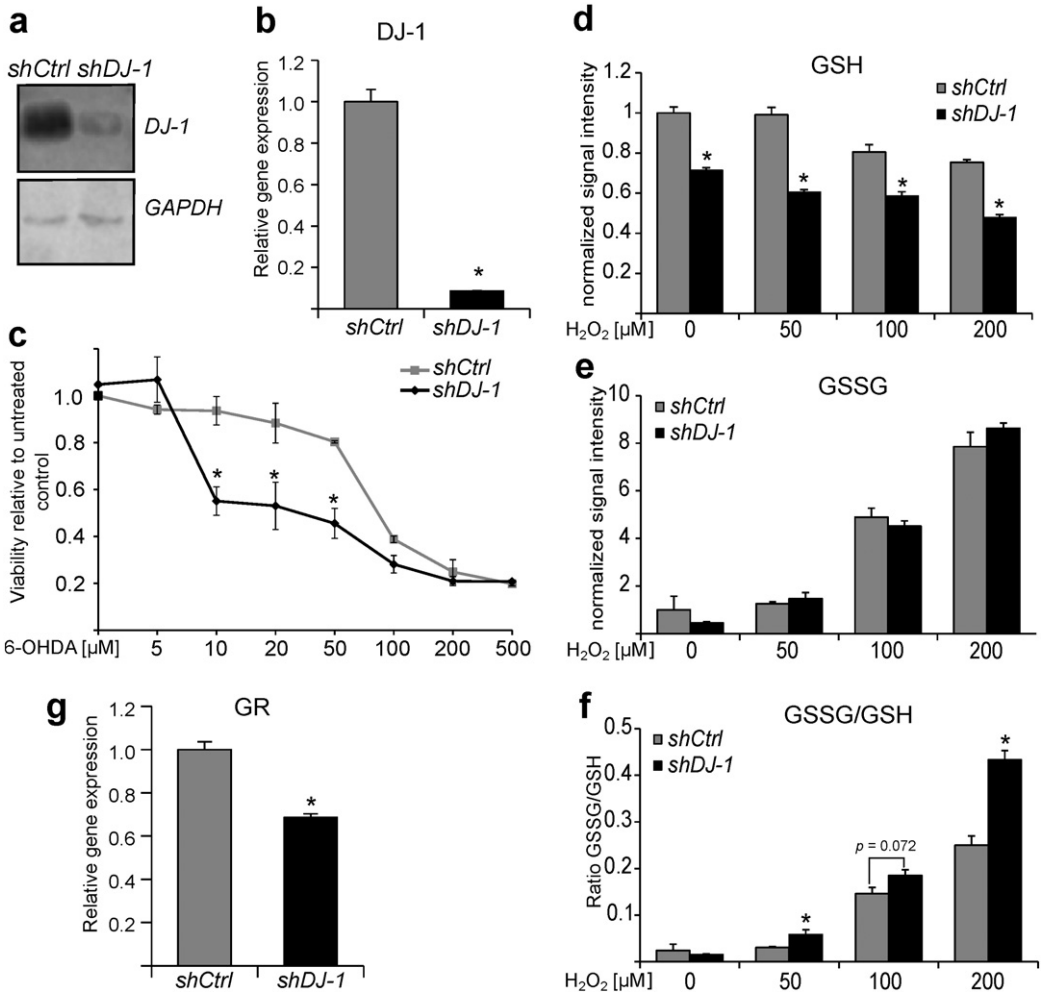

Fig. 1. Loss of *DJ-1* increases sensitivity to oxidative stress and affects glutathione homeostasis. (a–b) Western blot and qPCR analysis demonstrating DJ-1 knockdown. (c) Viability assay of LUHMES cells in response to oxidative stress. Cells were treated for six hours with different concentrations of 6-hydroxydopamine (6-OHDA). (d–e) Relative quantification of (d) GSH and (e) GSSG, 20 min after treatment with H_2O_2. (f) Ratio GSSG/GSH. (g) Gene expression of *GR*. Error bars represent SEM. Asterisks indicate a significant difference to the respective *shCtrl* (Welch's *t*-test, $p < 0.05$; number of biological replicates: $n \geq 3$). See also Supplementary Fig. S1.

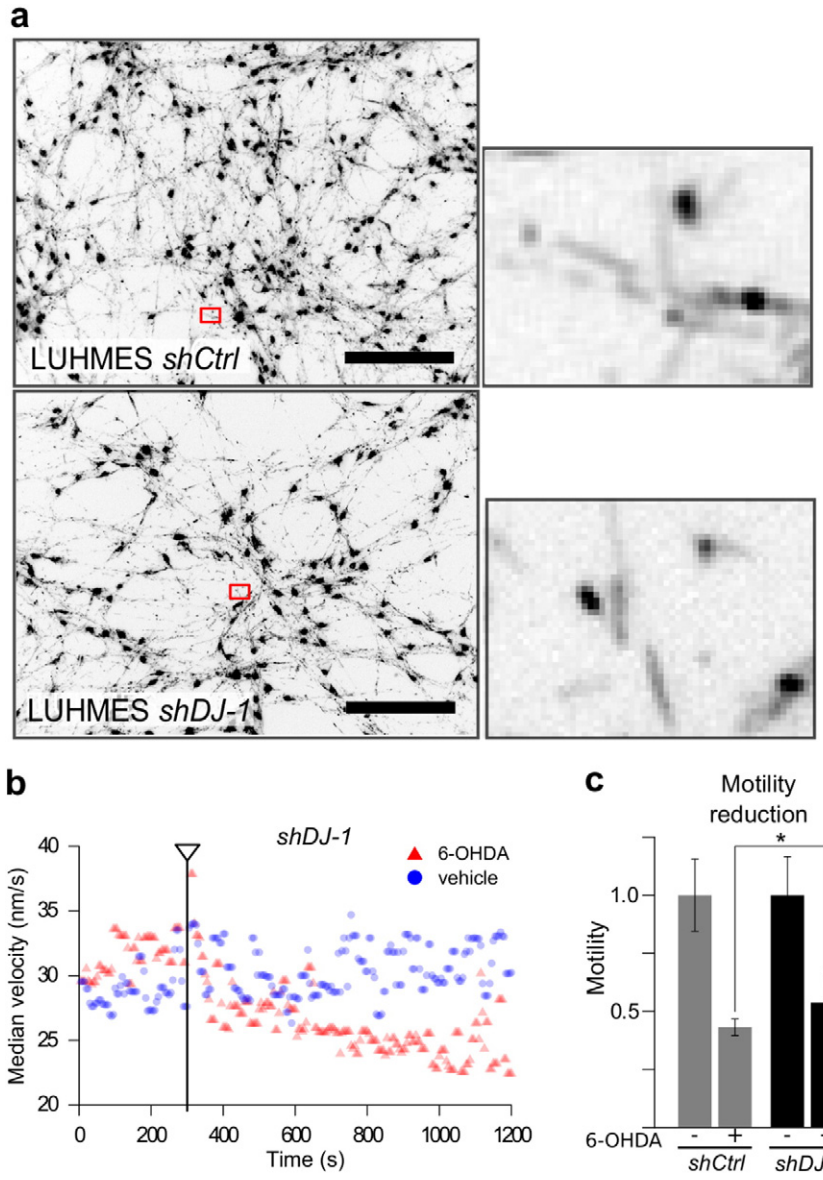

Fig. 2. Loss of DJ-1 affects mitochondrial motility in neurons (a) Fluorescence microscopy image of differentiated LUHMES cells stained with TMRM (scale bar = 100 μM) and a 10× magnification of a selected area (red square). Stain shows the location of mitochondria in soma and neurites. (b) Representative time-course of global mitochondrial motion analysis (in this case *shDJ-1*). Before and after (300 s; grey bar) addition of 200 μM 6-OHDA. Mito motility was reduced due to addition of 6-OHDA (red) compared to control (blue). (c) Parallel measurement of global mitochondrial motion. Shown values were normalized to the mean velocity measured before treatment with 6-OHDA. Error bars in (c) represent SD. Asterisks indicate a significant difference to the respective *shCtrl* cells (Student's *t*-test, $p < 0.05$ number of biological replicates $n = 3$). See also Supplementary movies and Fig. S2.

decreased viability (within the range of 10–50 μM 6-OHDA) compared to *shCtrl*, confirming that loss of DJ-1 increases sensitivity to oxidative stress.

To further analyze the cellular response to ROS, we measured the level of reduced (GSH) and oxidized (GSSG) glutathione after H_2O_2 treatment by UHPLC–MS (Fig. 1d–f). Already without any additional perturbation, GSH levels in *shDJ-1* cells were lower than in the respective *shCtrl* cells. With increasing concentrations of H_2O_2, we detected decreasing GSH levels and a concomitant increase of GSSG and thus an increase in the GSSG/GSH ratio. The GSSG/GSH ratios were more increased in *shDJ-1* cells, pointing to insufficient GSH regeneration from GSSG or a lack of alternative detoxification mechanisms. In line with these observations, we also found decreased gene expression levels of *glutathione reductase* (*GR*) in DJ-1 deficient cells (Fig. 1g).

Insufficient ROS detoxification is likely to affect mitochondrial integrity (Irrcher et al., 2010; Kahle et al., 2009). In neurons, mitochondria are actively transported through the projections of neuronal cells to directly satisfy axonal and synaptic energy demands (Saxton and Hollenbeck, 2012). Therefore, we investigated whether *shDJ-1* cells exhibit systematically different mitochondrial motion patterns than *shCtrl* cells and whether loss of the gene function would elicit different responses upon 6-OHDA treatment. To that end, we monitored the global motion of fluorescence-stained mitochondria in differentiated LUHMES cells by time-lapse microscopy (Fig. 2, Supplementary Movies and Fig. S2). Without perturbation, there was no significant difference in mitochondrial movement between the two cell types (Fig. 2C).

Consistent with the literature (Chen et al., 2008) we observed a general deceleration of mitochondrial motion in both cell types, following 6-OHDA treatment (Fig. 2b). Surprisingly, deceleration showed a trend to be less in *shDJ-1* cells compared to *shCtrl* cells (Fig. 2c and Supplementary movies and Fig. S2), suggesting that the regulation of mitochondrial transport in response to 6-OHDA-mediated oxidative stress might be affected by loss of DJ-1.

Together with the observation that the treatment did not lead to a significant drop of the mitochondrial membrane potential in the two cell types (Supplementary Movies) this may indicate additional effects of the induced oxidative stress. A direct target would be Ca^{2+} homeostasis (Guzman et al., 2010) that in turn can influence mitochondrial trafficking by Miro1 (Stephen et al., 2015; Nguyen et al., 2014) and TCA cycle activity by polarization (Krols et al., 2016). Furthermore, DJ-1 deficiency is associated with an impaired microtubule dynamics (Sheng et al., 2013) leading to modified cytoskeleton structures that can affect mitochondrial transport.

2.2. Loss of DJ-1 affects central metabolism

To investigate if the observed moderate changes in mitochondrial motility may have an impact on the cellular energy pool, we profiled cellular metabolism by determining uptake and release rates and by analyzing intracellular fluxes using stable isotope labeled tracers. We detected a decrease in alanine release in *shDJ-1* cells (Fig. 3a), whereas differences in glucose, pyruvate and serine consumption and lactate release were not statistically different (Fig. 3b, c, d, e). This reduction in alanine release of shDJ-1 cells, suggests a lower requirement for nitrogen excretion in these cells.

Since shDJ-1 cells are more sensitive to oxidative stress, we investigated if the canonical NADPH producing pathways, the pentose phosphate pathway and the folate mediated one-carbon metabolism are affected. To this end, we analyzed gene expression of *glycine dehydrogenase* (*GLDC*), the rate-limiting enzyme of the glycine cleavage system, of *glucose-6-phosphate dehydrogenase* (*G6PDH*), the rate-limiting enzyme of the PPP and of 5,10-*methylene tetrahydrofolate* (THF) *dehydrogenase* (*MTHFD*), a key enzyme in folate metabolism. We did not observe significant changes in the expression of *GLDC*, but decreased expression of *G6PDH*, *MTHFD1* and *MTHFD2* (Fig. 3f–h, S3), pointing to decreased carbon flux into these pathways and decreased cellular potential to generate NADPH, needed for antioxidative activities.

To monitor metabolic fluxes through glycolysis, the serine biosynthesis pathway, glycine cleavage and through PDH, we used uniformly labeled ^{13}C glucose as a tracer. We found that relative glucose contribution to serine biosynthesis was decreased in *shDJ-1* cells (Fig. 3j), which is in line with the observed decreased expression of MTHFD1/2. The trend of increased serine uptake (p-value = 0.084) might be a consequence of the decreased biosynthetic flux from glucose. Furthermore, based on M2 citrate isotopologues we did not observe any difference in relative glucose oxidation through PDH (Fig. 3k; 3I for atom transitions), suggesting that not glucose oxidation, but serine and folate metabolism are dependent on DJ-1.

DJ-1 has been shown to stabilize NRF2 in cancer cells (Clements et al., 2006). NRF2 is a key transcription factor that regulates cellular antioxidant responses also by activating serine flux and folate-mediated one-carbon metabolism (Mitsuishi et al., 2012). However, by Western Blotting we were unable to detect NRF2 in LUHMES cells (Fig. S3f). Concluding from non-detectable NRF2 levels in LUHMES cells, it is possible

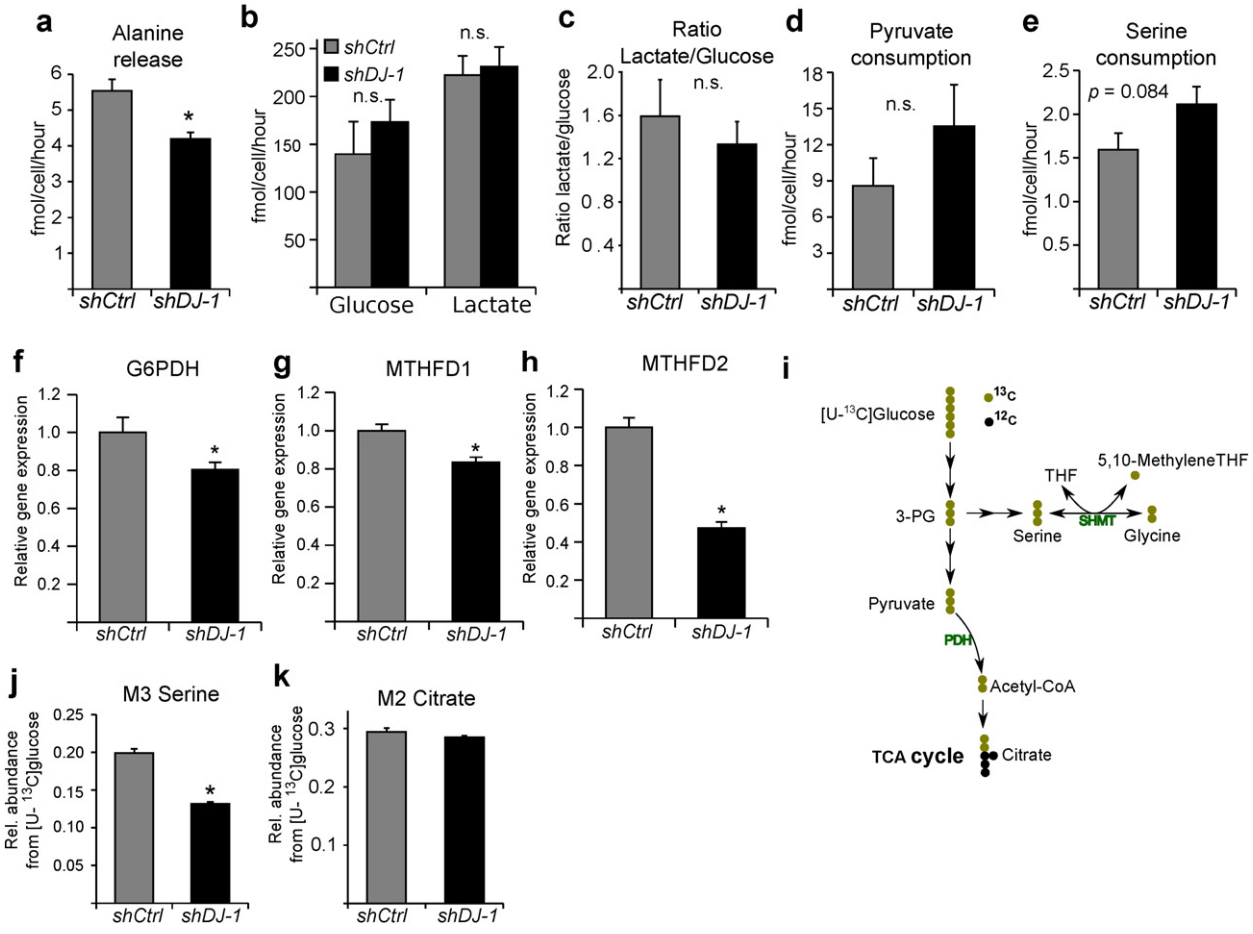

Fig. 3. Metabolic profiling of *DJ-1* silenced LUHMES cells reveals decreased serine biosynthesis flux. (a) Medium consumption and release rates of (a) alanine (release) (b) glucose and lactate. (c) Ratio lactate release/glucose consumption. (d–e) Consumption rates of (d) pyruvate and (e) serine. (f–h) Gene expression (qPCR) of (f) *G6PDH* (g) *MTHFD1* and (h) *MTHFD2*. (i) Schematic of atom transitions in central metabolism using [U-^{13}C]glucose as a tracer. ^{13}C carbons are in green, ^{12}C in black. (j–k) Application of [U-^{13}C]glucose as a tracer in LUHMES cells for determination of MIDs to infer relative intracellular fluxes. (j) M3 serine isotopologue indicating relative serine biosynthesis flux. (k) M2 citrate isotopologue indicating relative PDH flux. Error bars represent SEM. Asterisks indicate a significant difference to the respective *shCtrl* (Welch's *t*-test, $p < 0.05$; number of biological replicates: $n \geq 3$). See also Supplementary Fig. S3.

that the role of DJ-1 in regulating neuronal metabolism in the context of cellular antioxidant responses is even more pronounced, compared to other cell types.

Next, we analyzed TCA cycle fluxes in more detail and we applied uniformly labeled glutamine as a tracer (Fig. 4a for atom transitions). Stable isotope labeling revealed decreased glutamine contribution to the intracellular glutamate pool and to the TCA cycle intermediates alpha-ketoglutarate (aKG), succinate, fumarate, malate, aspartate (as a proxy of oxaloacetate) and citrate (Fig. 4b and c). Analysis of glutamine consumption indicated decreased uptake in *shDJ-1* cells (p-value = 0.057) (Fig. 4d). Moreover, we observed decreased gene expression of *glutaminase 2* (*GLS2*) (Fig. 4e), suggesting decreased glutamine-based anaplerosis. To evaluate the importance of glutamine as a carbon source, we calculated its relative carbon contribution to aKG and citrate (Fig. 4f). Providing 45% of carbon to aKG in *shCtrl*, glutamine represents the major precursor of aKG, highlighting the importance of this amino acid to central metabolism. In *shDJ-1*, glutamine carbon contribution to aKG and citrate was significantly lower than in *shCtrl*, which is in line with our finding of decreased glutamine uptake in *shDJ-1*. Interestingly, we found, that not the contribution of glucose, but that of other carbon sources increased to compensate for the lack of glutamine. Therefore, we quantified the consumption of branched chain amino acids (BCAAs), because their catabolism produces anaplerotic acetyl-coA and succinyl-coA. We observed that the uptake of these three amino acids was indeed elevated in *shDJ-1* cells compared to *shCtrl* (Fig. 4g).

In conclusion, an increased uptake of BCAAs may compensate for the decreased glutamine carbon contribution, but does not prevent increased sensitivity to oxidative stress, which therefore, seems to depend more specifically on serine metabolism and the supply of cysteine via the transsulfuration pathway to generate GSH. Moreover, since glutamine has additional roles in metabolism such as to provide nitrogen for the synthesis of nucleotides it is possible that lack of glutamine represents an additional perturbation to the cell, which makes it more prone to collapse.

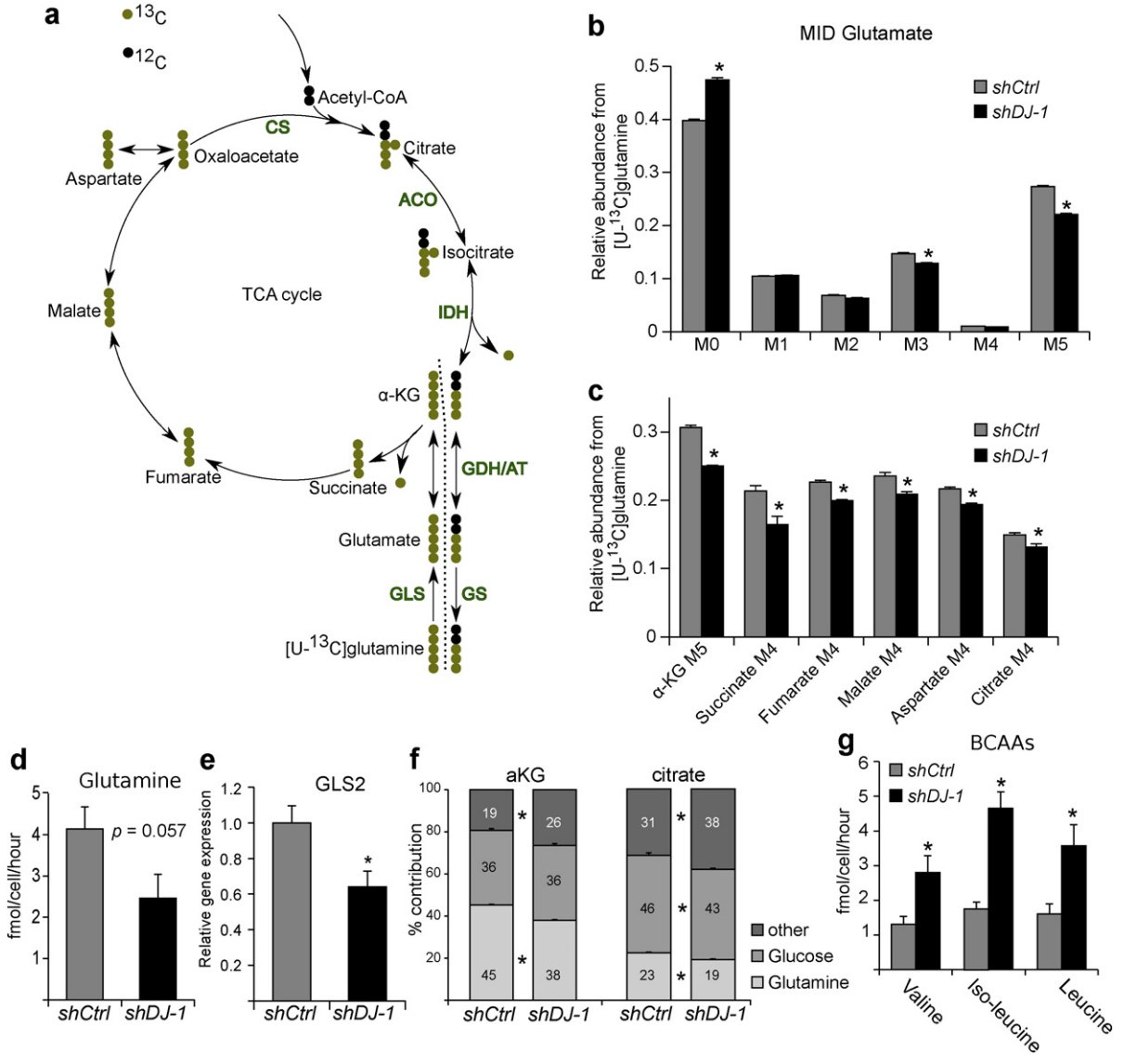

Fig. 4. Metabolic profiling of *DJ-1* silenced LUHMES cells reveals decreased glutamine influx. (a) Schematic of atom transitions in central metabolism using [U-^{13}C]glutamine as a tracer. ^{13}C carbons are in green, ^{12}C in black. ACO: aconitase; AT: aminotransferase; CS: citrate synthase; GDH: glutamate dehydrogenase; GLS: glutaminase; GS: glutamine synthetase; IDH: isocitrate dehydrogenase. The dotted line indicates beginning and end of one cycle. (b–c) Application of [U-^{13}C]glutamine as a tracer in LUHMES cells for determination of MIDs to infer relative intracellular fluxes. (b) MID of glutamate. (c) Relative abundance of M5 aKG, M4 succinate, M4 fumarate, M4 malate, M4 aspartate and M4 citrate. (d) Glutamine consumption from the medium. (e) Gene expression of *GLS2*. (f) Carbon contribution of glucose, glutamine and other carbon sources (%) to aKG and citrate. (g) Branched chain amino acid consumption. Error bars represent SEM. Asterisks indicate a significant difference to the respective *shCtrl*. (Welch's t-test, $p < 0.05$; number of biological replicates: $n \geq 3$). See also Supplementary Fig. S4.

2.3. Loss of DJ-1 affects mitochondrial metabolism but does not impair TCA cycle activity

Loss of DJ-1 is often discussed in the context of mitochondrial dysfunction (Clements et al., 2006; Ariga et al., 2013; Irrcher et al., 2010; Kahle et al., 2009; Krebiehl et al., 2010), but how, and more importantly, to what extent this dysfunction manifests on a pathophysiological level remains to be further specified. A strong inhibition of oxidative phosphorylation (OxPhos) caused by ROS would be detrimental for persons carrying a loss of function mutation in *DJ-1*. To analyze this hypothesis in more detail, we inspected TCA cycle activity. In case of OxPhos inhibition, NADH can no longer be oxidized by complex I of the respiration chain, which results in an increased NADH/NAD^+ ratio. This altered ratio leads to a thermodynamic shift of IDH activity, resulting in increased reductive carboxylation of aKG (Fendt et al., 2013; Mullen et al., 2014; Wegner et al., 2015). When using [U-$^{13}C_5$]glutamine as a tracer, this inhibition manifests in increased relative abundance of M5 citrate isotopologues, while the relative abundance of M4 citrate isotopologues, decreases (Fig. 5A). To test the effect of OxPhos inhibition and to compare this effect with the metabolic phenotype of *shDJ-1* cells, we treated the cells with MPP^+, an inhibitor of complex I of the electron transport chain, specifically taken up by DAergic neurons through the DA transporter (Javitch et al., 1985; Schildknecht et al., 2015).

Upon MPP^+ treatment, we observed a significant increase in fully labeled glutamate and M5 citrate in both cell lines (Fig. 5b, c). As expected, the oxidative route of the TCA cycle was inhibited upon MPP^+ treatment, and therefore, relative abundance of M4 citrate was strongly reduced. Although reductive IDH flux was induced in MPP^+-treated *shDJ-1* cells, M5 labeling of citrate and glutamate was lower in *shDJ-1*, originating from decreased relative glutamine influx into the TCA cycle. This decrease was also reflected in higher abundances of unlabeled citrate and glutamate as well as in lower M3 glutamate (Fig. 5b, c). Interestingly, compared to shDJ-1, we did not observe a decrease in M0 citrate upon MPP^+ treatment in *shCtrl* cells (Fig. 5c). To normalize for the decreased glutamine influx we analyzed the ratio of M5 citrate/M5 glutamate, indicating reductive carboxylation of aKG, M4 citrate/M5 glutamate, indicating glutamine oxidation and M5 citrate/M4 citrate, indicating the ratio of reductively to oxidatively derived citrate from fully labeled glutamine (Fig. 5d–f). These ratios confirmed a strong induction of reductive IDH flux upon MPP^+-treatment in both cell lines. However, there was no significant difference between the two cell types.

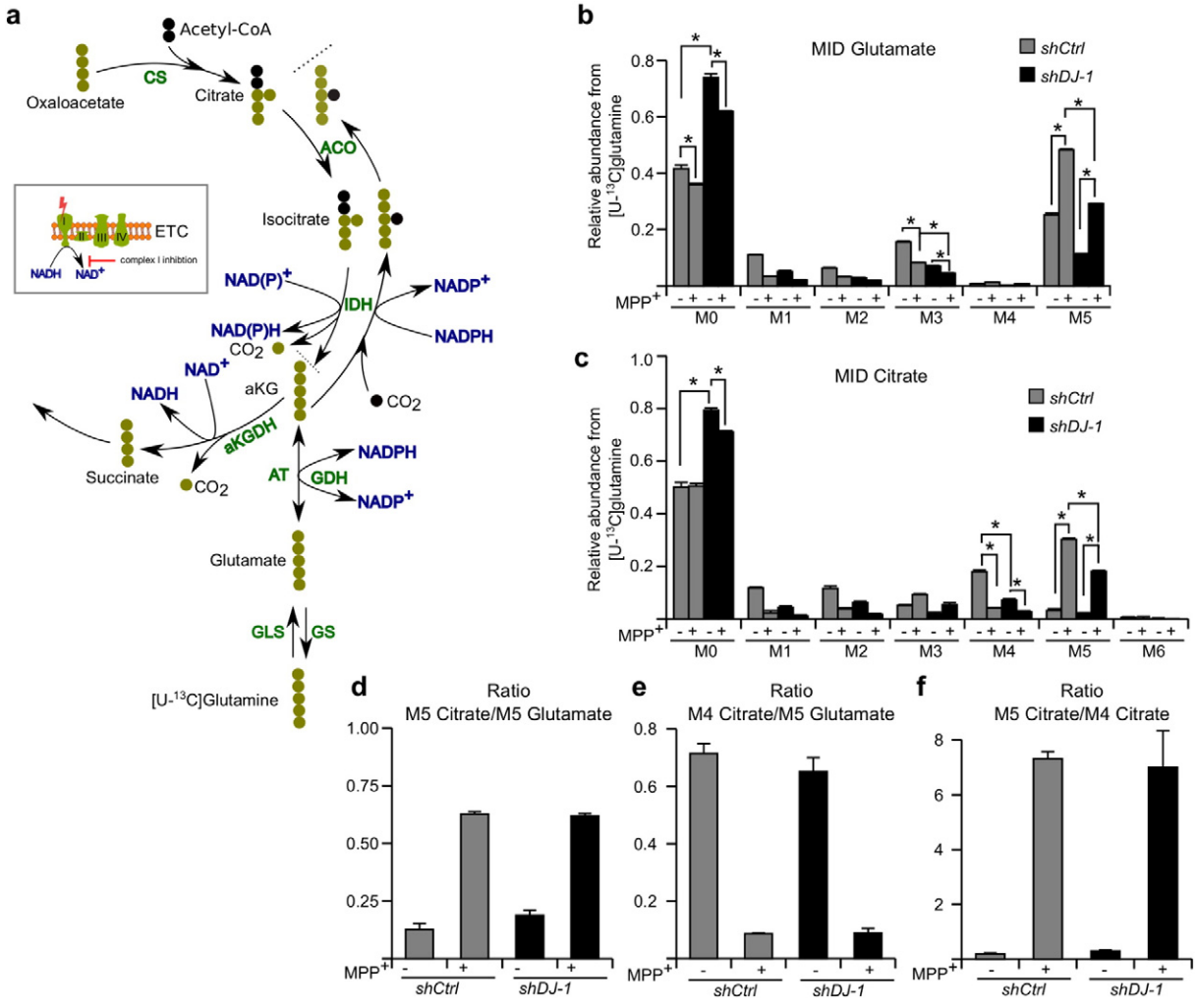

Fig. 5. *DJ-1* silenced LUHMES cells show an active TCA cycle but suffer from decreased glutamine contribution. (a) Schematic of atom transitions in central carbon metabolism using [U-^{13}C]glutamine as a tracer. Shown is reductive carboxylation of M5 aKG to M5 citrate via IDH and ACO. The specific isoenzyme depends on the compartment and is not further considered. For abbreviations see Fig. 4. The dotted line indicates end of one route. In case of complex I inhibition at the electron transport chain (ETC), NADH can no longer be oxidized which leads to a thermodynamic shift in the IDH reaction. (b–c) Application of [U-^{13}C]glutamine as a tracer in LUHMES cells for determination of MIDs to infer relative intracellular fluxes. (b) MID of glutamate. (c) MID of citrate. (d–f) Ratios of (d) M5 citrate/M5 glutamate, indicating reductive carboxylation of aKG (e), M4 citrate/M5 glutamate, indicating oxidation of aKG (f), M5 citrate/M4 citrate, indicating the ratio of reductive to oxidative route. LUHMES *shDJ-1* and *shCtrl* cells were treated with 10 μM MPP^+ for 6 h. Error bars represent SEM. Asterisks indicate a significant difference to the respective *shCtrl* (two-way ANOVA, $p < 0.05$; number of biological replicates: $n = 3$).

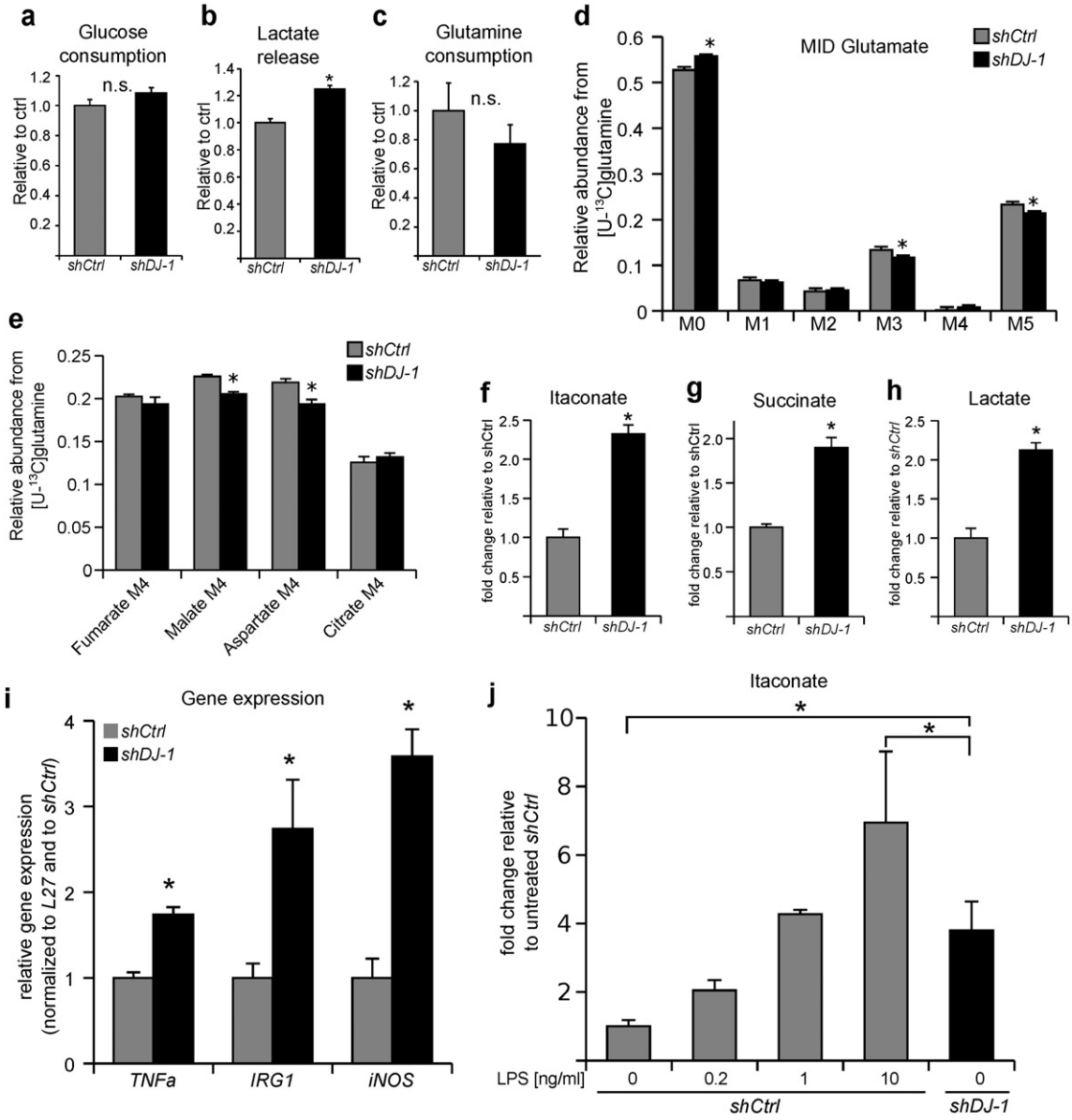

Fig. 6. *Dj-1* silencing affects glutamine metabolism in the mouse microglia cell model BV-2 and causes pro-inflammatory activation. (a–c) Medium consumption and release rates of (a) glucose, (b) lactate and (c) glutamine. (d–e) Application of [U-^{13}C]glutamine as a tracer in BV-2 cells for determination of MIDs to infer relative intracellular fluxes. (d) MID of glutamate. (e) Relative abundance of M4 fumarate, M4 malate, M4 aspartate and M4 citrate. (f–h) Intracellular metabolite levels of itaconate (f), succinate (g) and lactate (h) in BV-2 *shDJ-1* cells compared to *shCtrl*. (i) Gene expression analysis of the inflammatory marker genes *TNFα*, *Irg1* and *iNOS*. (j) Intracellular itaconate levels in *shDJ-1* and *shCtrl* cells. *shCtrl* cells were treated for 6 h with LPS. Error bars represent SEM. Asterisks indicate a significant difference to the respective *shCtrl* (Welch's *t*-test, $p < 0.05$; number of biological replicates: $n = 3$). See also Supplementary Fig. S5.

Analysis of MPP$^+$ treated LUHMES cells leads to the following three conclusions: (1) Lack of DJ-1 does not result in inhibition of OxPhos. Therefore, the general potential to produce ATP via NADH oxidation is still present in DJ-1 deficient cells. (2) The metabolic fate of glutamine between the oxidative and the reductive route is not different between the two cell types upon MPP$^+$ treatment. (3) As a consequence of loss of *DJ-1*, glutamine influx into the TCA cycle is decreased. Whether or not this is solely a result of elevated ROS levels in DJ-1 deficient cells, or if this is rather a mechanistic consequence, needs to be studied further.

2.4. Loss of Dj-1 affects central metabolism in mouse microglia and is sufficient to trigger pro-inflammatory activation

Since neuronal integrity in the central nervous system (CNS) also relies on surrounding glia cells, we investigated the effect of *Dj-1* silencing in the mouse microglia cell line BV-2 (Fig. S5) (Blasi et al., 1990; Henn et al., 2009).

First, we were interested if the observed metabolic alteration in neuronal cells also occurs in microglia. We did not observe significantly increased glucose consumption but a 20% increase in lactate release (Fig. 6a–b). Although glutamine uptake seemed to be decreased in DJ-1 deficient cells, this difference was not significant (Fig. 6c). Stable isotope labeling of glutamine revealed decreased glutamate labeling in *shDJ-1* BV-2 cells (Fig. 6d). However, the difference in isotopic enrichment was not as pronounced as in LUHMES cells and was only significantly different in the case of malate, aspartate and glutamate (Fig. 6e). Overall, proliferating BV-2 cells showed similar alterations than observed in LUHMES cells but less pronounced.

Recently, it has been reported that loss of Dj-1 leads to increased pro-inflammatory (M1) activation of microglia and astrocytes after perturbation with activating compounds such as the toll like receptor

agonist LPS or the cytokine IFNγ (Kim et al., 2013; Trudler et al., 2014; Waak et al., 2009). In this study we wanted to investigate if solely the lack of Dj-1 is already sufficient to trigger M1 polarization, and thus, could be relevant in the context of neuroinflammation. We analyzed levels of the metabolic M1 markers succinate and itaconate (Michelucci et al., 2013; Strelko et al., 2011; Tannahill et al., 2013) as well as expression of *TNFα* and *iNOS*. We observed that a lack of Dj-1 function increased itaconate and succinate levels without an additional perturbation (Fig. 6f, g, S5). Furthermore, we observed increased intracellular lactate levels, most probably a combined result of both, lack of Dj-1 and M1 polarization (Fig. 6h).

To validate the activation, we analyzed gene expression levels of the pro-inflammatory marker genes *Irg1*, *iNOS* and *TNFα*. *Irg1* codes for the enzyme (Cad) that catalyzes the synthesis of itaconate from *cis*-aconitate (Michelucci et al., 2013; Degrandi, 2009; Hall et al., 2013). The increased level of itaconate correlates with a more than twofold increased *Irg1* gene expression in *shDJ-1* compared to *shCtrl*. Moreover, we observed that *TNFα* gene expression was increased twofold and that *iNOS* was more than three times higher expressed than in *shCtrl* (Fig. 6i). To evaluate, how the detected itaconate level in *shDJ-1* cells correlates with different levels of LPS stimulation, we activated the *shCtrl* cells with 0.2 ng, 1 ng and 10 ng of LPS (Fig. 6j). We observed that *shDJ-1* BV-2 microglia constitutively synthesize itaconate amounts corresponding to an activation of *shCtrl* cells with approximately 1 ng of LPS. Since we use 10 ng of LPS to mimic a full activation *in vitro*, we conclude that *shDJ-1* cells show a moderate but constitutive activation.

2.5. Loss of DJ-1 leads to a metabolic shift in primary human and murine immune cells

To validate the observed metabolic alterations in primary cells, we isolated bone marrow-derived cells of *Dj-1* knock-out (KO) mice and differentiated them into macrophages (BMDMs). Since DJ-1 is ubiquitously expressed (Nagakubo et al., 1997), we expected to find the observed metabolic changes also in non-CNS cell types. In line with our previous results in BV-2 cells, BMDMs of *Dj-1* KO mice produced more lactate (Fig. 7a). Moreover, BMDMs of *Dj-1* KO mice consumed significantly less glutamine compared to wild type (WT) BMDMs (Fig. 7B).

Additionally, we applied [U-^{13}C]glutamine as a tracer and observed decreased M5 glutamate fractions in Dj-1 KO cells (Fig. 7c). However, isotopic enrichment in other TCA cycle related metabolites (Fig. 7d) was not significantly different. Compared to LUHMES cells, these differences in isotopic enrichment might be caused by fundamental differences in carbon utilization between the two cell types and/or in a species-specific manner. Although each cell type shows also specific differences, overall, the uptake and release rates of glutamine and lactate point in the same direction when comparing LUHMES, BV-2 and BMDM cells. It is not surprising that cell type specific differences lead to different metabolic phenotypes. However, it is appealing that loss of DJ-1 shows a similar picture in these various cell types.

To further validate our findings, we were interested in analyzing human samples directly originating from patients carrying a *DJ-1* mutation. We analyzed cellular metabolism of peripheral blood derived mononuclear cells (PBMCs)-derived CD14$^+$ macrophages from four patients carrying homozygous and heterozygous loss of function mutations (c.192G > C) in the *DJ-1* gene (Hering et al., 2004). PBMCs are relatively easy to access and could therefore be used as a model in subsequent clinical trials. As controls, we analyzed three independent healthy controls. We applied [U-^{13}C]glucose to provide flux information for both, glycolysis and TCA cycle. Analysis of isotopic enrichment revealed that serine biosynthesis in CD14$^+$ macrophages was close to zero (Fig. S6a). However, the labeling pattern of glutamate showed increased relative abundance of M2 isotopologues in patient-derived macrophages carrying a *DJ-1* mutation (Fig. 7e, f, S6b), indicating increased relative glucose carbon contribution to the TCA cycle and to glutamate. This increase can be a consequence of lower glutamine influx, resulting in higher relative ^{13}C labeling from glucose. We also observed a relative increase of M2 glutamate in LUHMES *shDJ-1* cells compared to *shCtrl* (Fig. S6c).

In summary, the analysis of human PBMCs indicated that metabolic changes initially observed in a cellular model of the CNS might be diagnosed from patient-derived primary blood cells. Further analyses will clarify if the observed flux changes are common for this mutation and if heterozygous patients show gene-dose dependent effects.

3. Discussion

In this study, we analyzed the metabolic impact of loss of DJ-1. We demonstrated that loss of DJ-1 affects central metabolism, specifically leading to (1) decreased glutamine uptake and decreased glutamine contribution to the TCA cycle, (2) decreased serine biosynthesis, (3) increased sensitivity to ROS and (4) weakly, but constitutively activated microglia. These metabolic alterations coincide with decreased cell survival upon oxidative stress, which may promote early onset of PD. We speculate that these changes are caused by increased sensitivity to ROS as a direct result of loss of DJ-1. Unlike cancer cells, we did not detect NRF2 protein in LUHMES wild type cells which leads us to the assumption that DJ-1 has a more fundamental role in neurons, compared to cancer cells, where NRF2 as a regulator of antioxidant responses is highly abundant (Clements et al., 2006). We conclude that insufficient ROS quenching in DJ-1 deficient neurons is due to decreased GSH levels as well as decreased activity of NADP-reducing enzymes within central metabolism. In line, we observed decreased expression of *G6PDH*, the rate-limiting enzyme of the PPP and decreased expression of MTHFD1 and 2, enzymes of the folate cycle and an alternative route for the generation of NADPH. Moreover, we measured decreased *GR* expression, which is in line with the lower GSH levels and an increased GSSG/GSH ratio upon hydrogen peroxide stress. In conclusion, loss of DJ-1 affects all pathways needed for GSH homeostasis.

DJ-1 has been shown to activate the expression of glutamate cysteine ligase, a key enzyme of GSH synthesis (Zhou and Freed, 2005). However, based on our gene expression analysis, GCLC and GCLM expression was not altered, at least not in LUHMES cells (Fig. S3g, h). We suggest that decreased levels of the rate limiting amino acid cysteine provoke the drop in GSH abundance by altering the net flux towards GSH (Richman and Meister, 1975; Lu, 2013).

Serine can act as a precursor for cysteine and glycine and serves at the same time as a carbon donor for folate-mediated one-carbon metabolism, which has recently been appreciated for its importance in maintaining the cellular NADPH pool (Fan et al., 2014). 5,10-methylene-THF can be oxidized by the NADP-dependent enzyme MTHFD. We observed a moderate, but significantly decreased expression of cytosolic *MTHFD1* and a more strongly decreased expression of mitochondrial *MTHFD2*. Together with glutamate, cysteine and glycine are the building blocks for *de novo* glutathione synthesis. We have demonstrated before that enzymes of serine and folate metabolism as well as the transsulfuration pathway are induced in human neurons upon oxidative stress (Krug et al., 2014). Intriguingly, in the DJ-1 knock-out model, that shows elevated levels of oxidative stress, we observed that serine biosynthesis is decreased and expression of both *MTHFD1* and *2* are reduced. Therefore, DJ-1 is likely to have an important regulatory function in serine and folate metabolism by supporting NADPH and GSH homeostasis. This is especially pronounced due to our observation of no detectable protein levels of NRF2 in post-mitotic neuronal cells. However, we do not exclude the possibility that *in vivo*, neurons are supported by NRF2 mediated protective mechanisms that are derived from surrounding glia cells (Kraft et al., 2004).

The third building block of GSH is glutamate, directly derived from glutamine via glutaminase. We showed that *shDJ-1* cells exhibit decreased *GLS2* expression and lower glutamine influx. The decreased glutamine influx is furthermore reflected in decreased alanine release, suggesting lower glutamine derived anaplerotic reactions. When less

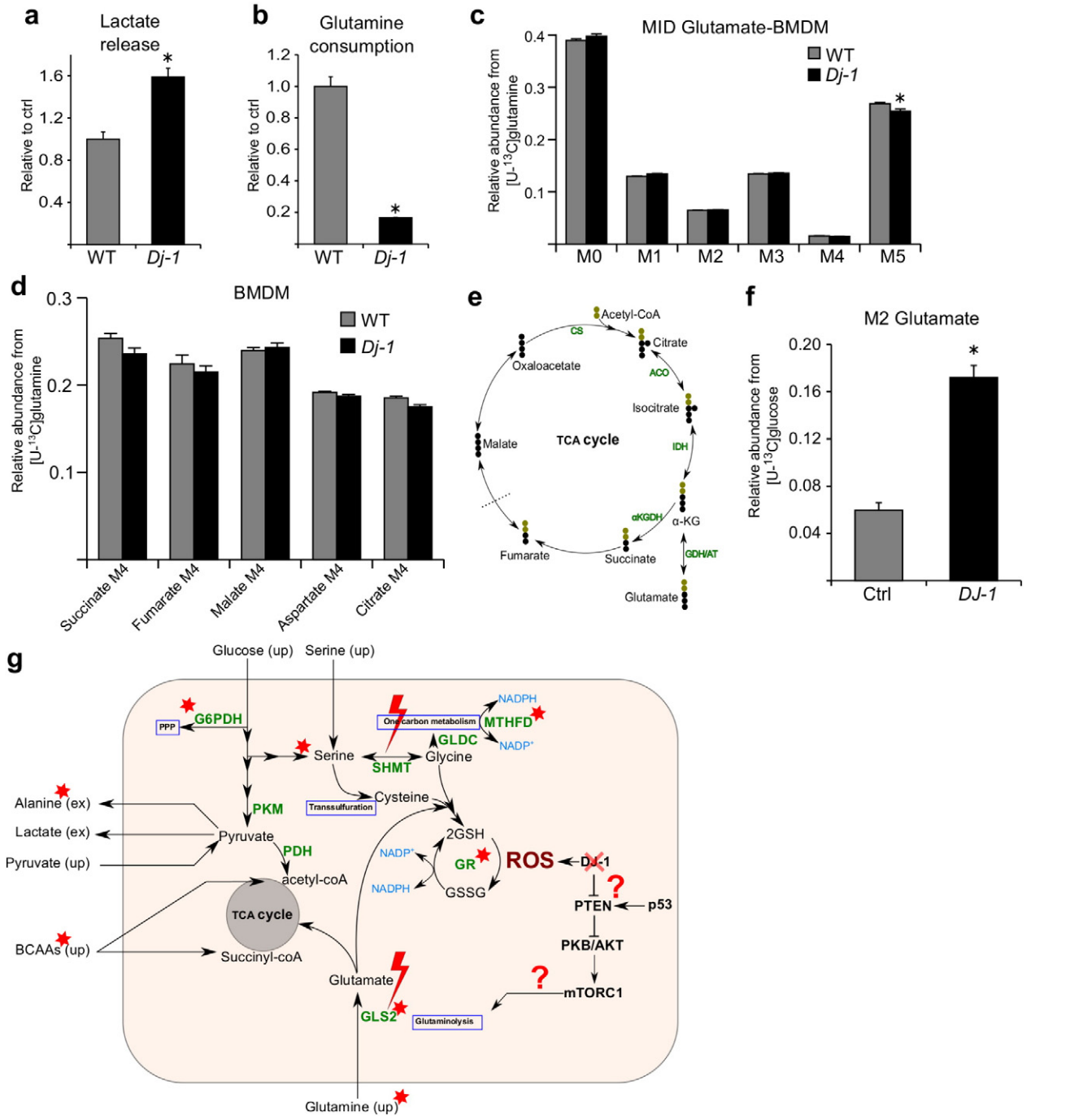

Fig. 7. Stable isotope labeling of BMDMs of *Dj-1* KO mice and PBMCs-derived $CD14^+$ macrophages of *DJ-1* patients indicate decreased glutamine contribution to the TCA cycle. (a) Relative lactate release of BMDMs. (b) Relative glutamine consumption of BMDMs. (c) MID of glutamate in BMDMs after application of [U-^{13}C]glutamine. (d) Relative abundance of M4 succinate, M4 fumarate, M4 malate, M4 aspartate and M4 citrate in BMDMs. Error bars represent SEM. Asterisks indicate a significant difference to the respective *shCtrl* (Welch's *t*-test, $p < 0.05$; number of biological replicates: $n = 5$). (e) Schematic of atom transitions in central carbon metabolism using [U-^{13}C]glucose. Illustrated is how M2 glutamate is generated from [U-^{13}C]glucose. The dotted line indicates end of one route. (f) Glutamate M2 isotopologue abundance of *DJ-1* subjects and non-familial healthy controls (Ctrl). Error bars represent SEM. The asterisk indicates a significant difference to the control (Welch's *t*-test, $p < 0.05$; number of individuals: $n \geq 3$). (g) Model highlighting the functional role of DJ-1 and summarizing the affected metabolic pathways as a result of DJ-1 deficiency. Affected metabolites, enzymes or pathways are highlighted with a red star. Loss of DJ-1 leads to decreased glutamine influx, decreased serine biosynthesis and decreased MTHFD expression, needed for glutathione (GSH) homeostasis and antioxidant response. Due to lower GSH levels, DJ-1 deficient cells show increased sensitivity to ROS. Additionally, lower expression of MTHFD and G6PDH suggests decreased potential to generate NADPH, needed for the reduction of GSSG. In cancer cells, DJ-1 acts as a repressor of PTEN, a negative regulator of AKT. Activated AKT can activate mTORC1. Both AKT and mTOR are important to drive metabolic processes needed for cell survival and proliferation, among others, glutaminolysis (for further explanation see discussion). Additionally, the transcription factor p53 can act as an activator on PTEN, thereby antagonizing DJ-1 function. Moreover, p53 can repress mTOR and introduces apoptosis. However, the relevance of these potential nodes of the metabolic network has to be further validated in neuronal cells. See also Supplementary Fig. S6.

glutamate enters the TCA cycle, less nitrogen has to be disposed from the cell. Previous work in cancer cell models demonstrated that a knock-down of *GLS2* results in decreased GSH levels and increased oxidative stress (Suzuki et al., 2010; Hu et al., 2010). However, Richman and Meister showed that not glutamate but cysteine is rate limiting to GSH synthesis (Richman and Meister, 1975). Therefore, we believe that serine and the adjacent transsulfuration pathway play an important role for the generation of GSH. On top of serine metabolism, decreased

expression of *GLS2* and lower glutamine influx adds an additional perturbation to the cell system, which ultimately triggers the observed physiological effects (Fig. 7g). The defect present in *shDJ-1* cells might not only be the result of elevated oxidative stress levels, but DJ-1 might play a role in additional processes. A possible role could be related to the described inhibitory function on PTEN (Kim et al., 2005). When DJ-1 is absent, AKT becomes hypophosphorylated (Aleyasin et al., 2010; Yang et al., 2005) and mTOR, a master regulator of anaplerosis, proliferation and cell survival, becomes less active, which could also favor the activity of p53. The transcription factor p53 is activated upon oxidative stress and can induce apoptosis (Vousden and Ryan, 2009). The role of these fundamental metabolic mechanisms is also relevant during neurogenesis (Rafalski and Brunet, 2011; Vasseur et al., 2009). However, the mechanistic link between DJ-1 and PTEN in regulating the AKT pathway is derived from cancer cells (Kim et al., 2005) and needs additional validation in post-mitotic neurons. Also the interplay between p53 and DJ-1 as well as the role of p53 in activating PTEN in neuronal non-proliferating cells needs additional research to gain a deeper understanding of the metabolic processes that are in place. Another potential link to the mTOR pathway is based on the work by Durán and colleagues (2012) who demonstrated that Rag-mTORC1 signaling is directly regulated by glutaminolysis and that a lack of glutamine results in less mTORC1 phosphorylation and less downstream activation without affecting ATP production (Durán et al., 2012). No difference in ATP production is also in line with our own results indicating functional OxPhos, a major pathway for ATP production, especially in neuronal cells. However, given the example of NRF2 abundance in LUHMES *versus* A549 lung cancer cells (Fig. S3f), comparisons with proliferating cancer cells should be interpreted carefully, since post-mitotic cells have very different metabolic requirements.

An apparent difference was also reflected by the lactate release in LUHMES cells and proliferating, immortalized BV-2 cells. In proliferating cells, increased ROS levels, as present in *shDJ-1* cells, can regulate PKM2 and enhance the Warburg effect. In its metabolically active form PKM2 acts as a tetramer. However, at increased ROS levels, PKM2 is post-translationally modified, stabilizing its dimeric or monomeric form (Anastasiou et al., 2011; Gupta and Bamezai, 2010; Lyssiotis et al., 2012). In this form, PKM2 translocates to the nucleus and influences transcriptional regulation to increase lactate release. In contrast to proliferating cells, post-mitotic neurons express the M1 isoform of pyruvate kinase (Tolle et al., 1976), which is less regulated (Anastasiou et al., 2012; Chaneton et al., 2012). This explains why we did not observe an increase in lactate fermentation in LUHMES cells, but increased lactate release in the proliferating (PKM2 expressing) BV-2 cells.

The reduction of glutamine influx after loss of DJ-1 was weaker in BV-2 cells than in post-mitotic LUHMES cells because BV-2 cells are immortalized with *v-myc*/*ras* (Blasi et al., 1990), which reprograms cellular metabolism to drive proliferation. A dependency of cancerous and proliferating cells on glutamine is well known (Wise and Thompson, 2010). Moreover, DJ-1 has been shown to activate ERK signaling, promoting cellular protection against oxidative stress (Gu et al., 2009). For that reason, immortalization with *v-myc*, an upstream regulator of ERK1/2 and AKT, might mask underlying metabolic defects by artificially activating the ERK pathway in DJ-1 deficient cells. Thus, the observed decreased glutamine influx and the known increased activation of PTEN due to lack of DJ-1 is at least partially overwritten in immortalized BV-2 cells, leading to re-elevated glutamine uptake. In differentiated LUHMES cells, *v-myc* expression is absent and is therefore not masking decreased glutamine influx (Scholz et al., 2011). Therefore, the metabolic dysfunction in differentiated, post-mitotic neurons is more pronounced and represents a clearer phenotype compared to BV-2 cells.

Besides the described effects in neurons, DJ-1 has been shown to play a role in inflammation by regulating cytokine expression and by interacting with STAT1 signaling (Kim et al., 2013; Trudler et al., 2014; Waak et al., 2009). Here, we demonstrated that solely the loss of DJ-1 results in weakly activated microglia. A constitutive, strong activation would cause immediate detrimental effects in a multicellular environment. However, a weak activation could be tolerated over a longer period of time (*e.g.* several years or decades) but would represent an additional trigger for PD, increasing the sensitivity of DAergic neurons over the course of life.

A metabolic reprogramming of immune cells upon M1 polarization has recently been described (Tannahill et al., 2013; Palsson-McDermott et al., 2015). M1 polarization in immune cells has been shown to induce a Warburg-like metabolic phenotype. A PKM2-mediated regulation in macrophages is possible (Palsson-McDermott et al., 2015). M1 polarized macrophages increase their rate of glycolysis and increase lactate release. In the case of loss of DJ-1, this is an additive effect and explains why the increase in lactate release is more pronounced in BV-2 cells compared to neurons. The metabolic adaptation to inflammation also includes increased glutamine oxidation in the TCA cycle (Tannahill et al., 2013). Therefore, decreased GLS2 activity in immune cells as a result of DJ-1 deficiency can at least be partially overwritten by inflammatory activation and immortalization.

Although TH^+-neurons do not proliferate, cellular survival and antioxidant response is even more important since these cells are mostly matured during embryogenesis and need to be functional over the whole life span to supply sufficient dopamine to the *striatum*. Increased oxidative stress during development can result in a lower absolute number of dopaminergic neurons in the midbrain (Pham et al., 2010). In conclusion, it becomes evident that as opposed to cancer therapy, where SHMT2 amplification drives oncogenesis (Kim et al., 2015; Lee et al., 2014) and where a decrease of glutamine uptake is a strategy to stop cell proliferation, a lack of glutamine influx and decreased serine biosynthesis flux seem to be part of the underlying metabolic problem in PD patients carrying a loss of function mutation in *DJ-1*.

4. Methods

4.1. Cell culture

Cells were standardwise tested for mycoplasma contamination in a rhythm of four to eight weeks.

4.2. LUHMES

Cells were kindly provided by the lab of Marcel Leist. Cells were grown in proliferation medium (Advanced DMEM/F12 + 1xN2 supplement (Invitrogen), 40 ng/ml FGF-2 and 2 mM glutamine) at 37 °C and 5% CO_2. Further cultivation and differentiation was performed as described in (Krug et al., 2014). For isotopic labeling, medium was replaced by differentiation medium containing 2 mM [U-$^{13}C_5$]glutamine or 17.5 mM [U-$^{13}C_6$]glucose. Cells were extracted at metabolic and isotopic steady state (42 h after labeling start). All experiments were performed with differentiated post-mitotic cells.

4.3. BV-2

Cells were kindly provided by the lab of Wolfgang Wurst. Cells were grown in DMEM (D5796) (Invitrogen) containing 5 mM glutamine, 25 mM glucose, 10% FBS and 1% P/S at 37 °C and 5% CO_2. For isotopic labeling medium was replaced by the same medium containing 5 mM [U-^{13}C]glutamine or 25 mM [U-^{13}C]glucose and dialysed FBS. Cells were extracted at metabolic and isotopic steady state (24 h after labeling start).

4.4. Extraction of intracellular metabolites

Cells were cultivated in 12-well plates and washed with 1 ml of 0.9% NaCl and quenched with 0.2 ml −20 °C methanol. After adding an equal volume of 4 °C cold water, cells were collected with a cell scraper and transferred to tubes containing 0.2 ml −20 °C chloroform. The extracts

were shaken at 1400 rpm for 20 min at 4 °C (Thermomixer Eppendorf) and centrifuged at 16,000 × *g* for 5 min at 4 °C. 0.2 ml of the upper aqueous phase was collected in specific glass vials with micro inserts and evaporated under vacuum at −4 °C using a refrigerated CentriVap Concentrator (Labconco).

4.5. Liquid chromatography–tandem mass spectrometry to measure GSH and GSSG

Cells were cultured in 12-well plates (500,000 cells per well) and washed once with 1× PBS before adding 40 μl of 5% TCA, followed by an equal volume of cold H_2O. 2 wells were pooled for one sample to increase abundance of GSSG in the sample. Cells were scraped, transferred into 1.5 ml Eppendorf tubes and centrifuged for 5 min at 13,000 × *g* at 4 °C. Supernatant was transferred into LC–MS glass vials with insert and stored at −80 °C until measurement. Measurement was performed using an Agilent 1290 Series LC coupled to an Agilent 6550 iFunnel Q-TOF MS system equipped with a Dual Agilent Jet Stream ESI source. The columns used in this study were a Waters ACQUITY UPLC HSS T3 1.8 μm (length, I.D., particle size: 100 mm × 2.1 mm × 1.8 μm) and a Phenomenex Kinetex 2.6 μm C18 100 A (length, I.D., particle size: 150 mm × 2.1 mm × 2.6 μm). The autosampler was kept at 4 °C and the column compartment at constant temperature of 45 °C. The LC conditions were optimized to achieve the best chromatographic parameters for both analytes. The flow rate was set to 0.3 ml/min and the mobile phases consisted of 0.1% formic acid in water (eluent A) and 0.1% formic acid in 60% methanol (eluent B). The run consisted of a isocratic delivery of 1% eluent B over 10 min, followed by a linear gradient to 99% eluent B over 2 min, isocratic delivery of 99% eluent B for 7 min, and a re-equilibration phase on starting conditions with 1% eluent B for 5 min. The eluent from the column was only introduced into the mass spectrometer within the first 10 min. The injection volume was 20 μl.

All the MS experiments were performed using electrospray ionization in positive mode (+ESI).

The identity of both GSH and GSSH were confirmed by MS/MS and standard addition experiments. Full scan spectra were acquired from *m/z* 150…1000 (1 spectra/s).

The protonated molecules of both GSH and GSSG were monitored in high resolution mode with following Q-TOF MS conditions: drying gas temperature: 225 °C, drying gas flow: 14 l/min (nitrogen), nebulizer: 35 psig, sheath gas temperature: 350 °C, sheath gas flow: 11 l/min, fragmentor: 400 V, skimmer: 65 V, Oct. RF Vpp: 750 V.

All data were acquired with Agilent MassHunter Workstation Software, version B.05.01 and analyzed with Agilent Qualitative Analysis, version B.06.00. Signal intensities were normalized to cell number.

4.6. Gas chromatography–mass spectrometry

Metabolite derivatization was performed using a Gerstel MPS. Dried polar metabolites were dissolved in 15 μl of 2% methoxyamine hydrochloride in pyridine at 40 °C under shaking. After 60 min an equal volume of MTBSTFA was added and held for 60 min at 40 °C. 1 μl sample was injected into an SSL injector at 270 °C in splitless mode. GC/MS analysis was performed using an Agilent 7890A GC equipped with a 30 m DB-35MS + 5 m Duraguard capillary column. Helium was used as carrier gas at a flow rate of 1.0 ml/min. The GC oven temperature was held at 100 °C for 2 min and increased to 300 °C at 10 °C/min. After 3 min, the temperature was increased to 325 °C. The GC was connected to an Agilent 5975C inert XL MSD, operating under electron ionization at 70 eV. The MS source was held at 230 °C and the quadrupole at 150 °C. The MS was operated in selected ion monitoring (SIM) (Table S1). The total run time of one sample was 25.00 min. All GC/MS chromatograms were processed by using MetaboliteDetector. MIDs were determined and corrected for natural isotope abundance using MetaboliteDetector (Hiller et al., 2009).

In case of absolute quantification of metabolites, a dilution series of a standard mix containing all relevant metabolites was included in the sequence and measured in duplicates.

Measurement of glucose and pyruvate intensities was performed by derivatization with an equal volume of MSTFA (instead of MTBSTFA) and held for 30 min at 40 °C under continuous shaking. 1 μl sample was injected into an SSL injector at 270 °C in split 10 mode. GC oven temperature was held at 90 °C for 1 min and increased to 300 °C at 15 °C/min for 8 min to 320 °C. The total run time of one sample was 24.3 min.

4.7. Quantification of amino acids

Quantification of amino acids was performed on an Agilent 1100 HPLC System equipped with a Diode Array Detector. Separation was carried out on a ZORBAX Amino Acid Analysis Column (150 × 4.6 mm, 5 μm) with a preceding ZORBAX Amino Acid Analysis Guard Cartridge (Agilent Technologies, Santa Clara, CA, USA) at 40 °C in gradient mode. The eluents used were 40 mM Na_2HPO_4 (pH 7.8, eluent A) and a mixture of Acetonitrile, Methanol and Water (45:45:10, eluent B). 0.02% sodium azide was added to eluent A to prevent microbial growth. Primary amines were automatically derivatized with ortho-phthalaldehyde (OPA) in borate buffer (0.4 N in water, pH 10.2) and diluted in eluent A prior to injection. The resulting OPA-derivatives were subsequently detected at 338 nm (10 nm bandwidth — reference wavelength: 390 nm, 20 nm bandwidth). All medium samples were diluted 1:1 with the internal standard L-2-aminobutyric acid (final concentration: 300 μM) to correct for deviations resulting from the derivatization-process. External calibration standards as well as reference media with known concentrations were measured with every run to determine sample concentrations and ensure stability of the analysis. Gradient profile: 1.9 min: 0% eluent B; 18.1 min: 57% eluent B; 18.6 min: 100% eluent B; 22.3 min: 100% eluent B; 23.2 min: 0% eluent B; 26 min: 0% eluent B.

4.8. cDNA synthesis and gene expression analysis

cDNA synthesis and qPCR was performed as previously described (Michelucci et al., 2013). Briefly, RNA was isolated from the interphase after extraction of metabolites, using the Quiagen RNAeasy Mini Kit. 0.5–1 μg RNA was used for cDNA synthesis using SuperScript III (Invitrogen), following the manufacturer's instructions. qPCR was performed using iQ SYBR Green Supermix (Bio-Rad) as manufacturer's instructions. PCR was carried out on a Light Cycler 480 (Roche). Data analysis was performed using the Roche analysis software. Gene expression was normalized to the housekeeping gene *L27*. Primer sequences are summarized in Table S2.

4.9. Lentivirus mediated shRNA gene silencing

For gene silencing of LUHMES cells, the destination vectors containing shRNA were ordered from Thermo Scientific (http://www.thermoscientificbio.com). Plasmids were amplified and purified by maxiprep in *Escherichia coli* and subsequently used for virus production in HEK298FT cells according to the manufacturer's protocol. Harvested virus was filtered using a 45 μM filter and precipitated with 1/5 volume of sterile PEG10000 over night at 4 °C. Concentrated virus was aliquoted in 10 μl and stored at −80 °C. For virus transduction 10 μl virus was added to 50,000 cells on day 1 and day 2. After medium change on day 3 cells were selected using 200 ng/ml puromycin. Correct concentration of puromycin was evaluated by a kill curve.

4.10. Western blot

For preparation of whole cell extract, 1×10^6 cells were harvested, washed with ice cold 1× PBS (Invitrogen/Life Technologies Europe BV

Belgium), lyzed in 1× M-PER®, Mammalian Protein Extraction Reagent (Thermo Scientific, Belgium) completed with 1× protease inhibitor cocktail (Complete®, Roche, Luxembourg) and further processed according to manufactures instructons. Bradford assay was used to measure the protein concentration (Bio-Rad Protein Assay Dye Reagent, Bio-Rad, Belgium). Proteins were separated by size using sodium dodecyl sulfate polyacrylamide gel elegrophoresis (SDS-PAGE, 15%) and transferred to an Immobilon-FL PVDF membrane (Merck Millipore) using the Mini-PROTEAN Tetra Cell and PowerPac Basic Power Supply (Bio-Rad, Belgium). The membrane was blocked in 5% non-fat milk in phosphate buffered saline (PBS)-Tween for 1 h at room temperature. Blots were incubated with primary antibodies: anti DJ-1 XP® Rabbit mAb (D29E5) (CellSignaling, Bioke, Netherlands) in 5% BSA in PBS-T (1:1000) for 1 h at room temperature. After incubation with primary antibody, membrane was washed with PBS-T and incubated for 1 h at room temperature with anti rabbit-HRP secondary antibody (1:10,000). For equal loading control of samples monoclonal anti-GAPDH-HRP (mouse) antibody (G9295, Sigma, Belgium), was probed in 5% non-fat milk in PBS-T for 1 h at room temperature. Visualization was done using the ECL Plus Western Blotting Detection System Kit (GE Healthcare, Netherlands).

4.11. Cell viability assay

Cell viability was assayed using Resazurin (Sigma Aldrich, R7017) (O'Brien et al., 2000). Briefly, resazurin, blue and non-fluorescent, is reduced to resorufin, pink and fluorescent, proportionally to the number of living cells. After 1 h incubation with 5 μg/ml resazurin (spiked in medium), fluorescence was measured with a Biotek Synergy Mx microplate reader coupled to the Gen5 software at the excitation wavelength of 570 nm and emission at 590 nm.

4.12. Cell imaging

Predifferentiated LUHMES cells were seeded at a density of 60 k cells/well in 96-well plates. After 96 h the cells were post-mitotic and had formed strongly connected networks. One hour prior to imaging experiments, the wells were carefully washed and filled with 100 μl fresh differentiation medium supplemented with 25 nM tetramethylrhodamine (TMRM) to fluorescently stain mitochondria. Plates were then incubated for 30 min at 37 °C, 5% CO_2, whereafter the medium was replaced by TMRM-free solution. Plates were kept for further 30 min at 37 °C, 5% CO_2. Time-lapse images were acquired on a Nikon Ti Eclipse inverted microscope with motorized stage (Nikon Corporation, Tokyo, Japan) and high intensity mercury short arc lamp with monochromator (Cairn Research, Kent, UK) enclosed in a bench top incubator. Fluorescence excitation filter was 540/15 and emission filter 620/60. Automatic microscope control, stage programming and acquisition were done using OptoMorph (Cairn Research, Kent, UK).

Two types of experiments were performed: i) longitudinal acquisition of a single well with one image taken every 2 s for 20 min, and ii) comparative parallel acquisition by switching between two neighboring wells using the motorized stage and taking images every 5 s for 30 min. Imaged wells were supplemented with 200 μM 6-OHDA or pure water for control after 5 min. Images were taken using a 20× air objective and an EXi Blue camera (Qimaging, Surrey, BC) with an exposure time of 350 ms and saved as 16-bit grayscale TIFFs in 1392 × 1040 px.

4.13. Global motion analysis

Global motion by particle image velocimetry (PIV) was analyzed, which quantifies correlations between pairs of time-lapse images and infers velocities of the image elements that give rise to differences. Microscopy images were contrast-normalized and converted to 8-bit grayscale using ImageMagick. Particle image velocimetry was performed using the OpenPIV toolbox (Taylor et al., 2010) in sliding windows of 16 × 16 px with 8 px overlap in both vertical and horizontal direction. Statistical analysis of resulting velocity fields and visualization of results was done in GNU R. Global motion was quantified by calculating median velocities over sliding windows spanning six acquisition frames to reduce impulse noise corruption from imaging artifacts. Average motion was assessed in acquisition windows 1 to 100 (pre-treatment) and 401 to 500 (post-treatment) for longitudinal measurements as well as 1 to 40 (pre-treatment) and 301 to 340 (post treatment) for parallel measurements. Significance of difference in motility reduction was assessed by pooling average velocities before and after treatment from all time-lapse experiments ($n = 3$) and performing Student's t-test on relative velocities, *i.e.*, normalized to untreated control. Propagation of uncertainty when normalizing velocities was taken into account.

4.14. BMDM isolation, cultivation and differentiation

4.14.1. Animals

For bone marrow-derived macrophages cultures, C57BL/6 *DJ-1* KO and age-matched C57BL/6 WT mice were obtained from the Helmholtz Zentrum München (Germany) from Dr. Daniela Vogt-Weisenhorn and Prof. Dr. Wolfgang Wurst. Per group, 5 mice were analyzed and from each mouse three independent samples were obtained. All animal work in Munich was carried out in accordance with the European Communities' Council Directive 2010/63/EU. All efforts were made to minimize animal suffering during the work. All protocols involving animal handling were approved by the committee for the Care and Use of Laboratory animals of the Government of Upper Bavaria, Germany. C57BL/6 mice (obtained from Charles River Germany) were group housed in individually ventilated type IIL cages (four mice per cage) and maintained on a 12 h/12 h light/dark cycle with food and water available *ad libitum*. All animal procedures in Luxembourg, such as handling and euthanasia, have been performed according to the Federation of European Laboratory Animal Science Associations (FELASA) guidelines for the use of animals in research, and were institutionally approved by the Luxembourg Centre for System Biomedicine animal user committee and authorized by the local governmental agencies (Ministry of Health, Ministry of Agriculture, chief veterinarian of the Luxembourg government).

4.14.2. Bone marrow-derived macrophages

Mice were deeply anesthetized by intraperitoneal injection of 50 mg/kg of ketamine hydrochloride and 5 mg/kg xylazine hydrochloride and bone marrows were isolated and cultured as previously described by Zhang and colleagues (Zhang et al., 2008). Briefly, bone marrow was flushed from femurs and tibias of five C57BL/6 DJ-1 KO and five age-matched C57BL/6 WT mice and the resultant cell suspension was passed through a 70 μm filter (Greiner Bio-One). After a 10 min centrifugation step at 250 ×*g*, supernatant was discarded and pellet re-suspended in 2 ml hypotonic solution (170 mM NH_4Cl) for 5 min to allow lysis of any remaining extracellular red blood cells. Bone marrow-derived cells were finally plated in 12-well plates (Greiner Bio-One) at 5×10^5 cells per well. Cells were cultured for 6 days in complete macrophage medium (Dulbecco modified Eagle's minimal essential medium DMEM) (Invitrogen) supplemented with 10% fetal bovine serum (FBS) (Invitrogen), 20% conditioned medium from macrophage-colony stimulating factor-secreting L929 fibroblasts and 1% penicillin/streptomycin (Invitrogen) at 37 °C. After 6 days in culture, adherent cells were approximately 95% pure macrophages and cells were used for experiments. Stable isotope tracers were added for 24 h prior extraction of intracellular metabolites.

Per genotype 5 individual mice were sacrificed and from each mouse three replicates of BMDMs were used for the analysis.

4.14.3. PBMC derived $CD14^+$ macrophages

The four *DJ-1* patients were brothers of one family (one homozygous and three heterozygous). The samples were analyzed in a blinded

study; patient samples were given numbers and were identified after the results were completely analyzed. The controls were non-family members with different genetic background (two male, one genotype unknown (blood donation from the red cross)). The $CD14^+$ cells were isolated by a positive selection method using the magnetic activated cell sorting (MACS) method: Blood samples of the patients were separated in 50 ml Leucosept tubes (Greiner) through Ficoll-Paque Premium (GE Healthcare) density gradient centrifugation (1000 × *g*) for 10 min at room temperature, using no break. After 30 min incubation at 4 °C with 2 μl of $CD14^+$ beads (Miltenyi biotech) per 10^7 PBMCs, the $CD14^+$ cells got purified using a positive LS column (Miltenyi Biotech). The purified $CD14^+$ cells were incubated for 24 h at 37 °C and 5% CO_2 in DMEM D5030 medium (Sigma) containing 11 mM [U-$^{13}C_6$]glucose and 5 mM glutamine for metabolite extraction. Cells were extracted at metabolic and isotopic steady state (24 h after labeling start, (tested before with other blood donations)). Heterozygous and homozygous patients were male, two healthy controls were male, the status of the third healthy control is unknown (blood donation of the red cross).

4.14.4. Statistical analyses

To analyze a significant difference between two groups, the Welch's *t*-test or two-way ANOVA was applied. The level of $p < 0.05$ was considered as significant different. Significance of difference in motility reduction was assessed by pooling average velocities before and after treatment from all time-lapse experiments ($n = 3$) and performing Student's *t*-test on relative velocities, *i.e.*, normalized to untreated control. Propagation of uncertainty when normalizing velocities was taken into account.

Supplementary data to this article can be found online at http://dx.doi.org/10.1016/j.nbd.2016.01.019.

Author contributions

JM planned and performed experiments, analyzed data and wrote the manuscript; SD performed experiments, analyzed data and provided parts of Fig. S3. AW and DW analyzed data and revised the manuscript; JG, XD, and LK performed experiments; SS performed and discussed experiments; AM isolated BMDMs; YN set up the HPLC method and measured medium samples; AF and AS performed microscopy and motility analysis; CJ developed LC–MS methods, measured and analyzed the GSH experiments; CS generated and validated BV-2 *shDJ-1* and BV-2 *shCtrl* cells; FG supervised virus production for BV-2 cells; OP tried to detect NRF2 protein via mass-spectrometry; JS helped to establish the method for the PBMCs experiments; RK helped with PBMCs experiment and revised the manuscript; DWo. takes care for DJ-1 patients and isolated blood of DJ-1 patients; DV-W and WW provided *Dj-1* KO mice and revised the manuscript; ML revised the manuscript and discussed experiments; KH planned and discussed experiments and revised the manuscript.

Competing financial interests

The authors declare no conflict of interest.

Acknowledgments

Related research of the authors was supported by the Fonds National de la Recherche (FNR) Luxembourg (ATTRACT A10/03 and AFR-Postdoc-3973022). We thank the laboratory of Prof. Paul Heuschling for mouse hosting and Dr. Eric Koncina and Dr. Manuel Buttini for expert help with bone marrow isolation. We thank Dr. Aidos Baumuratov from the LCSB Imaging Facility for assistance and technical support with the microscopes. This work was funded (in part) by the Helmholtz Alliance ICEMED — Imaging and Curing Environmental Metabolic Diseases, through the Initiative and Network Fund of the Helmholtz Association (WW), and the Helmholtz Portfolio Themes 'Metabolic Dysfunction and Common Disease' (CS, DMVW) and 'Supercomputing and Modelling for the Human Brain' (SMHB) (FG). We also thank Dr. Dietrich Trümbach and Artem Romanov for critical input.

References

Aleyasin, H., et al., 2010. DJ-1 protects the nigrostriatal axis from the neurotoxin MPTP by modulation of the AKT pathway. Proc. Natl. Acad. Sci. 107, 3186–3191.
Anastasiou, D., et al., 2011. Inhibition of pyruvate kinase M2 by reactive oxygen species contributes to cellular antioxidant responses. Science 334, 1278–1283.
Anastasiou, D., et al., 2012. Pyruvate kinase M2 activators promote tetramer formation and suppress tumorigenesis. Nat. Chem. Biol. 8, 839–847.
Antony, P.M.A., Diederich, N.J., Krüger, R., Balling, R., 2013. The hallmarks of Parkinson's disease. FEBS J. 280, 5981–5993.
Ariga, H., et al., 2013. Neuroprotective function of DJ-1 in Parkinson's disease. Oxidative Med. Cell. Longev. 2013, 1–9.
Bader, V., Ran Zhu, X., Lübbert, H., Stichel, C.C., 2005. Expression of DJ-1 in the adult mouse CNS. Brain Res. 1041, 102–111.
Baulac, S., et al., 2009. Increased DJ-1 expression under oxidative stress and in Alzheimer's disease brains. Mol. Neurodegener. 4, 12.
Blasi, E., Barluzzi, R., Bocchini, V., Mazzolla, R., Bistoni, F., 1990. Immortalization of murine microglial cells by a v-raf/v-myc carrying retrovirus. J. Neuroimmunol. 27, 229–237.
Bonifati, V., 2003. Mutations in the DJ-1 gene associated with autosomal recessive early-onset parkinsonism. Science 299, 256–259.
Bonifati, V., et al., 2003. DJ-1 (PARK7), a novel gene for autosomal recessive, early onset parkinsonism. Neurol. Sci. 24, 159–160.
Brown, G.C., Neher, J.J., 2010. Inflammatory neurodegeneration and mechanisms of microglial killing of neurons. Mol. Neurobiol. 41, 242–247.
Canet-Avilés, R.M., et al., 2004. The Parkinson's disease protein DJ-1 is neuroprotective due to cysteine-sulfinic acid-driven mitochondrial localization. Proc. Natl. Acad. Sci. U. S. A. 101, 9103–9108.
Chaneton, B., et al., 2012. Serine is a natural ligand and allosteric activator of pyruvate kinase M2. Nature 491, 458–462.
Chen, S., Owens, G.C., Edelman, D.B., 2008. Dopamine inhibits mitochondrial motility in hippocampal neurons. PLoS One 3, e2804.
Clements, C.M., McNally, R.S., Conti, B.J., Mak, T.W., Ting, J.P.-Y., 2006. DJ-1, a cancer- and Parkinson's disease-associated protein, stabilizes the antioxidant transcriptional master regulator Nrf2. Proc. Natl. Acad. Sci. 103, 15091–15096.
Davidson, B., et al., 2008. Expression and clinical role of DJ-1, a negative regulator of PTEN, in ovarian carcinoma. Hum. Pathol. 39, 87–95.
Degrandi, 2009. The proinflammatory cytokine-induced IRG1 protein associates with mitochondria. 29, 55–68.
Durán, R.V., et al., 2012. Glutaminolysis activates Rag-mTORC1 signaling. Mol. Cell 47, 349–358.
Fan, J., et al., 2014. Quantitative flux analysis reveals folate-dependent NADPH production. Nature 510, 298–302.
Fendt, S.-M., et al., 2013. Reductive glutamine metabolism is a function of the α-ketoglutarate to citrate ratio in cells. Nat. Commun. 4.
Gu, L., et al., 2009. Involvement of ERK1/2 signaling pathway in DJ-1-induced neuroprotection against oxidative stress. Biochem. Biophys. Res. Commun. 383, 469–474.
Gupta, V., Bamezai, R.N.K., 2010. Human pyruvate kinase M2: A multifunctional protein. Protein Sci. 19, 2031–2044.
Guzman, J.N., et al., 2010. Oxidant stress evoked by pacemaking in dopaminergic neurons is attenuated by DJ-1. Nature 468, 696–700.
Hall, C.J., et al., 2013. Immunoresponsive gene 1 augments bactericidal activity of macrophage-lineage cells by regulating β-oxidation-dependent mitochondrial ROS production. Cell Metab. 18, 265–278.
Hayes, J.D., Dinkova-Kostova, A.T., 2014. The Nrf2 regulatory network provides an interface between redox and intermediary metabolism. Trends Biochem. Sci. 39, 199–218.
Henn, A., et al., 2009. The suitability of BV2 cells as alternative model system for primary microglia cultures or for animal experiments examining brain inflammation. ALTEX 26, 83–94.
Hering, R., et al., 2004. Novel homozygous p. E64D mutation in DJ1 in early onset Parkinson disease (PARK7). Hum. Mutat. 24, 321–329.
Hiller, K., et al., 2009. MetaboliteDetector: comprehensive analysis tool for targeted and nontargeted GC/MS based metabolome analysis. Anal. Chem. 81, 3429–3439.
Hu, W., et al., 2010. Glutaminase 2, a novel p53 target gene regulating energy metabolism and antioxidant function. Proc. Natl. Acad. Sci. 107, 7455–7460.
Irrcher, I., et al., 2010. Loss of the Parkinson's disease-linked gene DJ-1 perturbs mitochondrial dynamics. Hum. Mol. Genet. 19, 3734–3746.
Javitch, J.A., D'Amato, R.J., Strittmatter, S.M., Snyder, S.H., 1985. Parkinsonism-inducing neurotoxin, N-methyl-4-phenyl-1,2,3,6-tetrahydropyridine: uptake of the metabolite N-methyl-4-phenylpyridine by dopamine neurons explains selective toxicity. Proc. Natl. Acad. Sci. 82, 2173–2177.
Kahle, P.J., Waak, J., Gasser, T., 2009. DJ-1 and prevention of oxidative stress in Parkinson's disease and other age-related disorders. Free Radic. Biol. Med. 47, 1354–1361.
Kim, R.H., et al., 2005. DJ-1, a novel regulator of the tumor suppressor PTEN. Cancer Cell 7, 263–273.
Kim, J., et al., 2013. DJ-1 facilitates the interaction between STAT1 and its phosphatase, SHP-1, in brain microglia and astrocytes: A novel anti-inflammatory function of DJ-1. Neurobiol. Dis. 60, 1–10.
Kim, D., et al., 2015. SHMT2 drives glioma cell survival in ischaemia but imposes a dependence on glycine clearance. Nature 520, 363–367.
Kraft, A.D., Johnson, D.A., Johnson, J.A., 2004. Nuclear factor E2-related factor 2-dependent antioxidant response element activation by tert-butylhydroquinone and

sulforaphane occurring preferentially in astrocytes conditions neurons against oxidative insult. J. Neurosci. 24, 1101–1112.
Krebiehl, G., et al., 2010. Reduced basal autophagy and impaired mitochondrial dynamics due to loss of Parkinson's disease-associated protein DJ-1. PLoS One 5, e9367.
Krols, M., et al., 2016. Mitochondria-associated membranes as hubs for neurodegeneration. Acta Neuropathol. (Berl.) http://dx.doi.org/10.1007/s00401-015-1528-7.
Krug, A.K., et al., 2014. Transcriptional and metabolic adaptation of human neurons to the mitochondrial toxicant MPP+. Cell Death Dis. 5, e1222.
Lee, J.-Yy., et al., 2012. Human DJ-1 and its homologs are novel glyoxalases. Hum. Mol. Genet. 21, 3215–3225.
Lee, G.Y., et al., 2014. Comparative oncogenomics identifies PSMB4 and SHMT2 as potential cancer driver genes. Cancer Res. 74, 3114–3126.
Lu, S.C., 2013. Glutathione synthesis. Biochim. Biophys. Acta Gen. Subj. 1830, 3143–3153.
Lyssiotis, C.A., et al., 2012. Cellular control mechanisms that regulate pyruvate kinase M2 activity and promote cancer growth. Biomed. Res. 23, 213–217.
Meiser, J., Weindl, D., Hiller, K., 2013. Complexity of dopamine metabolism. Cell Commun. Signal. 11.
Michelucci, A., et al., 2013. Immune-responsive gene 1 protein links metabolism to immunity by catalyzing itaconic acid production. Proc. Natl. Acad. Sci. 110, 7820–7825.
Mitsuishi, Y., et al., 2012. Nrf2 redirects glucose and glutamine into anabolic pathways in metabolic reprogramming. Cancer Cell 22, 66–79.
Mitsumoto, A., Nakagawa, Y., 2001. DJ-1 is an indicator for endogenous reactive oxygen species elicited by endotoxin. Free Radic. Res. 35, 885–893.
Mullen, A.R., et al., 2014. Oxidation of alpha-ketoglutarate Is required for reductive carboxylation in cancer cells with mitochondrial defects. Cell Rep. 7, 1679–1690.
Nagakubo, D., et al., 1997. DJ-1, a novel oncogene which transforms mouse NIH3T3 cells in cooperation with ras. Biochem. Biophys. Res. Commun. 231, 509–513.
Nguyen, T.T., et al., 2014. Loss of Miro1-directed mitochondrial movement results in a novel murine model for neuron disease. Proc. Natl. Acad. Sci. U. S. A. 111, E3631–E3640.
O'Brien, J., Wilson, I., Orton, T., Pognan, F., 2000. Investigation of the Alamar Blue (resazurin) fluorescent dye for the assessment of mammalian cell cytotoxicity. Eur. J. Biochem. 267, 5421–5426.
Palsson-McDermott, E.M., et al., 2015. Pyruvate kinase M2 regulates hif-1α activity and IL-1β induction and is a critical determinant of the Warburg effect in LPS-activated macrophages. Cell Metab. 21, 65–80.
Pham, T.T., et al., 2010. DJ-1-deficient mice show less TH-positive neurons in the ventral tegmental area and exhibit non-motoric behavioural impairments. Genes Brain Behav. 9, 305–317.
Rafalski, V.A., Brunet, A., 2011. Energy metabolism in adult neural stem cell fate. Prog. Neurobiol. 93, 182–203.
Richman, P.G., Meister, A., 1975. Regulation of gamma-glutamyl-cysteine synthetase by nonallosteric feedback inhibition by glutathione. J. Biol. Chem. 250, 1422–1426.
Saxton, W.M., Hollenbeck, P.J., 2012. The axonal transport of mitochondria. J. Cell Sci. 125, 2095–2104.
Schildknecht, S., et al., 2015. Preferential extracellular generation of the active parkinsonian toxin MPP(+) by transporter-independent export of the intermediate MPDP(.). Antioxid. Redox Signal. 23, 1001–1016.
Scholz, D., et al., 2011. Rapid, complete and large-scale generation of post-mitotic neurons from the human LUHMES cell line. J. Neurochem. 119, 957–971.
Sheng, C., et al., 2013. DJ-1 deficiency perturbs microtubule dynamics and impairs striatal neurite outgrowth. Neurobiol. Aging 34, 489–498.
Stambolic, V., et al., 1998. Negative regulation of PKB/Akt-dependent cell survival by the tumor suppressor PTEN. Cell 95, 29–39.
Stephen, T.-L., et al., 2015. Miro1 regulates activity-driven positioning of mitochondria within astrocytic processes Apposed to synapses to regulate intracellular calcium signaling. J. Neurosci. 35, 15996–16011.
Strelko, C.L., et al., 2011. Itaconic acid is a mammalian metabolite induced during macrophage activation. J. Am. Chem. Soc. 133, 16386–16389.
Sun, H., et al., 1999. PTEN modulates cell cycle progression and cell survival by regulating phosphatidylinositol 3,4,5,-trisphosphate and Akt/protein kinase B signaling pathway. Proc. Natl. Acad. Sci. U. S. A. 96, 6199–6204.
Suzuki, S., et al., 2010. Phosphate-activated glutaminase (GLS2), a p53-inducible regulator of glutamine metabolism and reactive oxygen species. Proc. Natl. Acad. Sci. 107, 7461–7466.
Tannahill, G.M., et al., 2013. Succinate is an inflammatory signal that induces IL-1β through HIF-1α. Nature 496, 238–242.
Taylor, Z.J., Gurka, R., Kopp, G.A., Liberzon, A., 2010. Long-duration time-resolved PIV to study unsteady aerodynamics. IEEE Trans. Instrum. Meas. 59, 3262–3269.
Tolle, S.W., Dyson, R., Newburgh, R., Cardenas, J.M., 1976. Pyruvate kinase isozymes in neurons, glia, neuroblastoma, and glioblastoma. J. Neurochem. 27, 1355–1360.
Trudler, D., Weinreb, O., Mandel, S.A., Youdim, M.B.H., Frenkel, D., 2014. DJ-1 deficiency triggers microglia sensitivity to dopamine toward a pro-inflammatory phenotype that is attenuated by rasagiline. J. Neurochem. 129, 434–447.
van der Brug, M.P., et al., 2008. RNA binding activity of the recessive parkinsonism protein DJ-1 supports involvement in multiple cellular pathways. Proc. Natl. Acad. Sci. 105, 10244–10249.
Van Duijn, C.M., et al., 2001. PARK7, a novel locus for autosomal recessive early-onset parkinsonism, on chromosome 1p36. Am. J. Hum. Genet. 69, 629–634.
Vasseur, S., et al., 2009. DJ-1/PARK7 is an important mediator of hypoxia-induced cellular responses. Proc. Natl. Acad. Sci. 106, 1111–1116.
Vousden, K.H., Ryan, K.M., 2009. p53 and metabolism. Nat. Rev. Cancer 9, 691–700.
Waak, J., et al., 2009. Regulation of astrocyte inflammatory responses by the Parkinson's disease-associated gene DJ-1. FASEB J. 23, 2478–2489.
Wegner, A., Meiser, J., Weindl, D., Hiller, K., 2015. How metabolites modulate metabolic flux. Curr. Opin. Biotechnol. 34, 16–22.
Wise, D.R., Thompson, C.B., 2010. Glutamine addiction: a new therapeutic target in cancer. Trends Biochem. Sci. 35, 427–433.
Yang, Y., et al., 2005. Inactivation of *Drosophila* DJ-1 leads to impairments of oxidative stress response and phosphatidylinositol 3-kinase/Akt signaling. Proc. Natl. Acad. Sci. U. S. A. 102, 13670–13675.
Yuen, H.-F., et al., 2008. DJ-1 could predict worse prognosis in esophageal squamous cell carcinoma. Cancer Epidemiol. Biomark. Prev. 17, 3593–3602.
Zhang, X., Goncalves, R., Mosser, D.M., 2008. The isolation and characterization of murine macrophages. Curr. Protoc. Immunol. http://dx.doi.org/10.1002/0471142735.im1401s83 (Chapter 14:Unit 14.1).
Zhou, W., Freed, C.R., 2005. DJ-1 up-regulates glutathione synthesis during oxidative stress and inhibits A53T α-synuclein toxicity. J. Biol. Chem. 280, 43150–43158.